Nuclear Inst. and Methods in Physics Research, A 987 (2021) 164835

Contents lists available at ScienceDirect

Nuclear Inst. and Methods in Physics Research, A

journal homepage: www.elsevier.com/locate/nima

# Design and fabrication of stripline BPM for the ESS MEBT

S. Varnasseri [a,*], I. Bustinduy [a], I. Rueda [a], R.A. Baron [b], A. Ortega [a], A. Zugazaga [a], A. Conde [a], J. Martin [a], T. Shea [b]

[a] ESS-Bilbao, Derio, Spain
[b] ESS ERIC, Lund, Sweden

ARTICLE INFO

*Keywords:*
Beam Position Monitor (BPM)
Stripline
MEBT
BPM transfer impedance

ABSTRACT

Beam Position Monitors (BPM) are non-destructive diagnostics devices used in particle accelerators to measure the transverse beam position (beam center of mass) and phase of the accelerated beam. There are various ways of realization of the BPMs in accelerators having different measurement requirements, particle type or energy. Several types of BPM pickups have been studied including the button type, grounded striplines and matched striplines. The choice and final design is based on a matched stripline to accommodate the signal transmission to electronics and provide relatively higher signal level for low velocity ($\beta = 0.088$) proton beam within MEBT. Due to mechanical space limits, all the BPMs are embedded inside quadrupoles; hence it is required to use non-magnetic materials in the BPM sensor, in particular the feedthroughs. The BPM sensor is composed of several components, which are separately machined with tolerances of 10 μm, and then welded together by the use of electron beam welding. The analysis show for long bunches, the multi bunch transfer impedance is different than of single bunch due to bunch signals overlapping. The design, fabrication and tests of the BPM sensors were performed at ESS-Bilbao and their installation and the electrical checks at ESS-Lund. Prior to installation in the ESS accelerator tunnel, one BPM stripline was installed and the BPM system tested with the CEA-IPHI beam. This paper gives an overview of the electromagnetic and mechanical design and the fabrication of BPM striplines. Furthermore, the results of the RF measurements are compared with the simulations.

## 1. Introduction

The European Spallation Source (ESS) Medium Energy Beam Transport (MEBT) is an accelerator section of the ESS Linear Accelerator (LINAC) under construction at Lund, Sweden [1–3]. Several beam diagnostics systems have been designed to monitor and characterize the 3.62 MeV beam parameters, which include systems for beam position and phase measurements [4,5]. There are overall 8 Beam Position Monitors (BPM) installed in the MEBT of ESS. All the BPM's are used for beam position and beam phase measurements and two of them are used for fast timing characterization (e.g. chopped beam rise time) and absolute beam energy measurements. Core design of sensors for the BPMs of MEBT is identical, however the electronics for position measurement and fast timing measurements are different. The electronic design is not discussed in this paper and is addressed in a separate paper [6]. As part of the beam diagnostics instruments necessary for commissioning and normal operation of accelerator; ESS-Bilbao has designed and manufactured eight stripline BPM sensors.

In Fig. 1, a view of MEBT during the pre-installation for required checks is shown. Out of eleven (11) quadrupoles of MEBT, eight (8) of them are housing the BPM pickups.

The proton beam has a nominal current of 62.5 mA, repetition frequency of 14 Hz, and pulse length of 2.8 ms, however its parameters will be changed in order to accommodate the various stages of commissioning and operation of the proton linac (e.g. reducing the beam current, pulse width and different modes) [7,8]. Various types of BPM pickups have been studied and analyzed in terms of their transfer impedance and signal amplitude at low energies. The button type, grounded stripline, open termination stripline and matched termination stripline are studied, and compared against the ESS MEBT characteristics, such as beam current, bunch length, RF frequency and beam energy. The BPMs are housed inside the quadrupoles due to the lack of longitudinal mechanical space in the MEBT (Fig. 2) [9]. The BPM main processing RF frequency for position measurement is 704 MHz to avoid crosstalk between the high power RF system that powers the RFQ and MEBT bunchers, which operate at the first harmonic, 352 MHz. The stripline output signal level, frequency response, sensitivity and mechanical restrictions are the main factors in the design of BPM sensors. Table 1 shows the main beam parameter related to BPM design analysis.

* Corresponding author.
*E-mail address:* svarnasseri@essbilbao.org (S. Varnasseri).

https://doi.org/10.1016/j.nima.2020.164835
Received 1 September 2020; Received in revised form 21 October 2020; Accepted 1 November 2020
Available online 4 November 2020

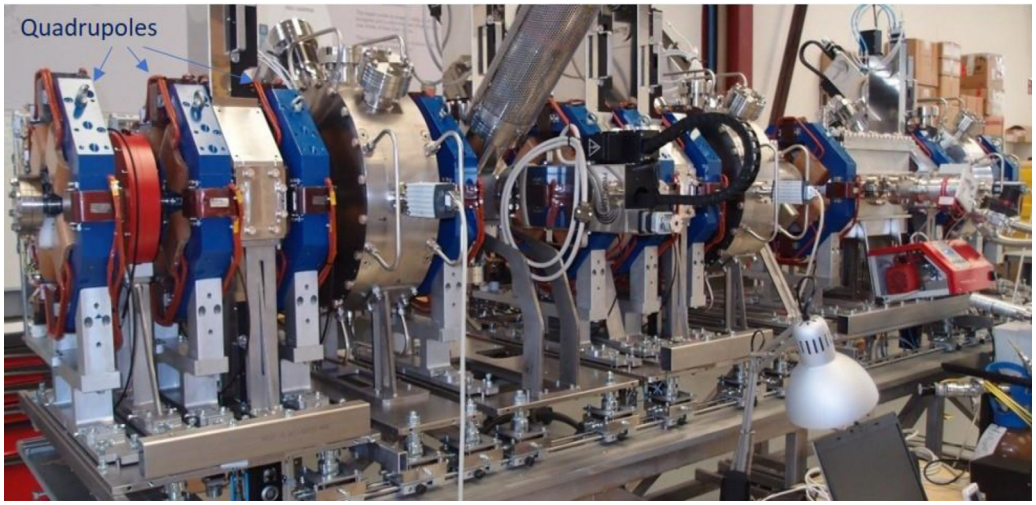


**Fig. 1.** The view of MEBT during pre-installation showing the location of BPMs in Quads.

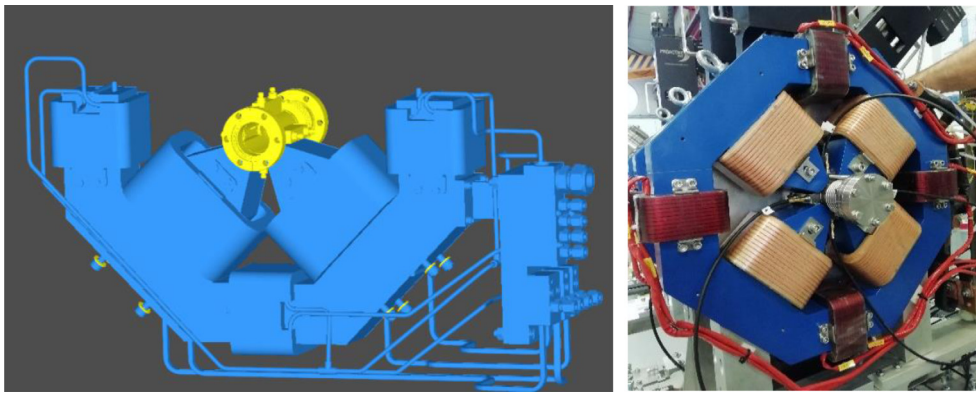

**Fig. 2.** A 3D cross section of the BPM housed inside quadrupole (left), and BPM signal cables connected for tests (right).

**Table 1**
Main BPM related beam parameters.

| Parameter | Value | Unit |
|---|---|---|
| Beam energy | 3.62 | MeV |
| Beam current (avg.) | 62.5 | mA |
| Particles/bunch | 1.1e9 | p |
| Readout frequency | 704 | MHz |
| RF frequency | 352 | MHz |
| Bunch length ($\sigma_z$) | 60–180 | ps |
| Pulse length (max.) | 2.86 | ms |
| Repetition rate | 14 | Hz |

## 2. Principle theory

Design of the BPM in the first stage is strongly limited by the beam characteristics and mechanical restrictions. These parameters include the beam current, bunch length, beam energy, readout frequency and the longitudinal space allowed inside the quadrupoles. The theoretical estimations of the BPM pickup output relation with the beam parameters is established by R.E. Shafer [10–12]. Considering a Gaussian bunch shape containing N particles of charge $e$ in a bunch rms temporal length of $\sigma$, then the beam current of a single bunch is given by:

$$I_b(t) = \frac{eN}{\sqrt{2\pi}\sigma} e^{\left(\frac{-t^2}{2\sigma^2}\right)} \tag{1}$$

Assuming a symmetric bunch shape in time with a bunching period of $T$, the repetitive beam current may be represented by a Fourier series expansion in the frequency domain as:

$$I_b(t) = \langle I_b \rangle + 2\langle I_b \rangle \sum_{n=1}^{\infty} A_n \cos(n w_0 t) \tag{2}$$

where:

$$A_n = e^{\left(\frac{-n^2 w_0^2 \sigma^2}{2}\right)} \tag{3}$$

And in which $\langle I_b \rangle$ is the average dc current, $w_o$ is the bunching angular frequency and $n$ is the harmonic number. For a bunch length of 0.18 *ns* in MEBT, $A_1$ and $A_2$ correspond to 0.924 and 0.728 for main and second harmonic of rf frequency.

Assuming a BPM with two opposite electrodes of angular width of $\phi$, one can estimate the image currents $I_R$ and $I_L$ on the BPM electrodes at angular frequency of $w$ for a moving off-center pencil beam at a distance of $r$ as [10]:

$$I_R = \frac{\sqrt{2}A_n \langle I_b \rangle \emptyset}{2\pi} \left[ \frac{I_0(gr)}{I_0(gb)} + \frac{4}{\emptyset} \sum_{m=1}^{\infty} \frac{1}{m} \frac{I_m(gr)}{I_m(gb)} sin\left[ m\left(\frac{\emptyset}{2} - \theta\right)\right]\right] \tag{4}$$

and

$$I_L = \frac{\sqrt{2}A_n \langle I_b \rangle \emptyset}{2\pi} \left[ \frac{I_0(gr)}{I_0(gb)} + \frac{4}{\emptyset} \sum_{m=1}^{\infty} \frac{1}{m} \frac{I_m(gr)}{I_m(gb)} sin\left[ m\left(\pi + \frac{\emptyset}{2} - \theta\right)\right]\right] \tag{5}$$

where $I_m(arg)$ represents the modified Bessel function of order m, and

$$g = \frac{\omega}{\beta\gamma c} \tag{6}$$

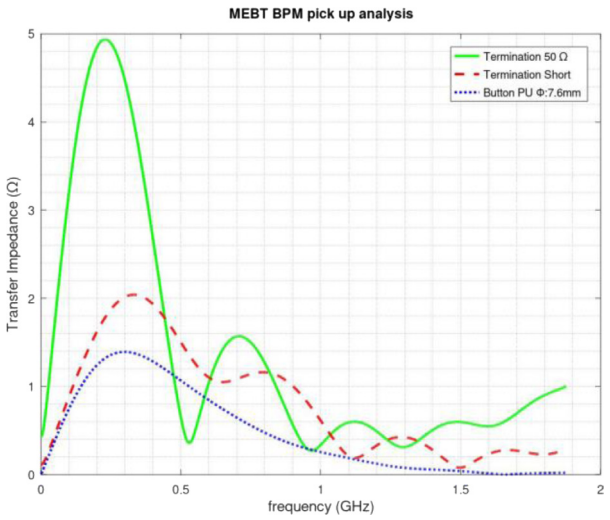


**Fig. 3.** Transfer Impedance comparison of the Button type and Stripline BPM.

In which $\gamma$ is the Lorentz contraction factor. A beam pipe with radius of $b$ around the moving off-center pencil beam with a velocity of $\beta c$ at distance of $r$ is considered.

From the above equations, one can derive that BPM electrode induced current is affected by the beam current, bunch shape or bunch frequency spectrum, beam energy and processing frequency. For the MEBT BPM the value of $g$ is equal to 167.5 $m^{-1}$, which corresponds to processing of second RF harmonic.

The value of the electrode current is an important factor of the $S/N$ ratio and consequently in the BPM position and phase measurements accuracy.

## 3. Comparison between BPM electrodes types

Since the BPMs are installed in the quadrupole magnetic field zone, the materials used in its structure must carry non-magnetic properties, to not affect the quadrupole magnetic field distribution within the magnet center axis. For the BPM pickups of MEBT, button type and various stripline types were studied. The 3D electromagnetic models of button type, short-end stripline and matched stripline are analyzed and the signal amplitude and transfer impedances are extracted from the results. Transfer impedance is defined as the $Z_t(f) = V_{PU}(f)/I_{beam}(f)$ which depends on the geometrical dimensions, type of the pickup and frequency. Fig. 3 shows the comparative calculated transfer impedance for stripline and button pickups. Considering the BPM signal power and quadrupole yoke geometry, the optimum dimensions for each type is evaluated. The BPM tube radius is 18.8 mm and the pickup width for the stripline and button is 7 mm and 7.6 mm respectively. In both cases the weldable SMA feedthrough with outer diameter of 9.48 mm, internal diameter of 7.72 mm and pin radius of 2.36 mm is modeled as the signal port. The analysis for transfer impedance shows absolute value of 1.6 Ω, 1.05 Ω and 0.65 Ω for matched stripline (solid line), shorted stripline (dashed line) and button pickups at processing frequency of 704 MHz (Fig. 3). The graph shows the higher transfer impedance of the matched stripline type and therefore higher signal to noise ratio of the beam position measurement for the proton beam of MEBT at the frequency of interest.

### 3.1. Multibunch signal power

Since thousands of consecutive bunches exist in a single MEBT beam pulse, the head and tail of induced signal of one bunch could overlap with the ones from adjacent bunches. The time domain analysis for the multi-bunch considering many consecutive bunches is performed and the voltage signal vs. time for a centered beam is shown in Fig. 4. The results are for the rms bunch size of 180 ps at energy $\beta = 0.088$ and RF frequency of 352.2 MHz. Fig. 4 shows an expected peak voltage amplitude of 290 mV at the output of the BPM striplines in multi-bunch pulses. However, the frequency of the resulting waveform is 352 MHz of RF, but the waveform is not a pure sine wave or Gaussian form of bunching frequency.

A comparative illustration of the frequency domain signal power for various configurations of the BPM pick-ups at RF harmonics is shown in Fig. 4. In these analyses many consecutive bunches are considered to evaluate the BPM output power at different harmonics of the RF frequency. With this approach the effects of positive/negative superposition of the consecutive bunch fields are implemented in the output power. In the comparative graphs, at the frequency spectrum from 352 MHz up to 5 GHz, the matched stripline (square symbol) produces larger RF power compared to short stripline (triangle symbol) and button pickups.

At the second harmonic of 704 MHz, the power values corresponding to matches stripline, short stripline and button pickups at the signal port of the BPM equals to −17.5 dBm,−20.4 dBm and −25.5 dBm accordingly. Resulting from these evaluations on transfer impedance, RF power amplitude and mechanical restrictions, we decided to utilize the 50 Ω matched BPM stripline type for the MEBT pickups.

In order to estimate the signal power budget out of the pick-ups, signal power simulations have been performed for multi-bunch pulses. It should be mentioned that Fig. 4 shows the time domain of the signal on the BPM port which includes several harmonics of frequency components of RF (i.e components of 352 MHz, 704 MHz and so on).

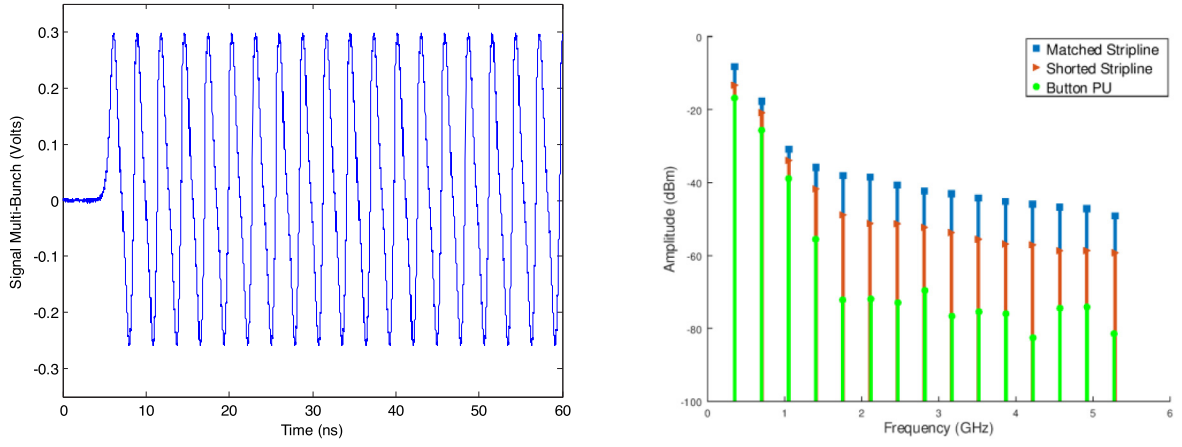


**Fig. 4.** Time and frequency domain multi-bunch expected signal on the stripline electrodes for nominal beam.

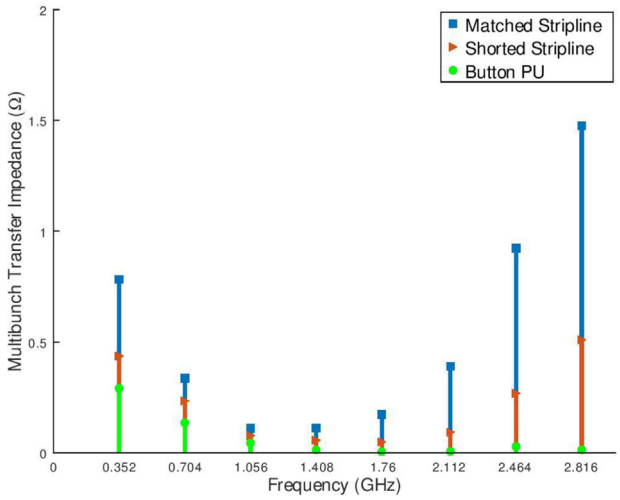


**Fig. 5.** Multibunch transfer impedance at RF harmonics.

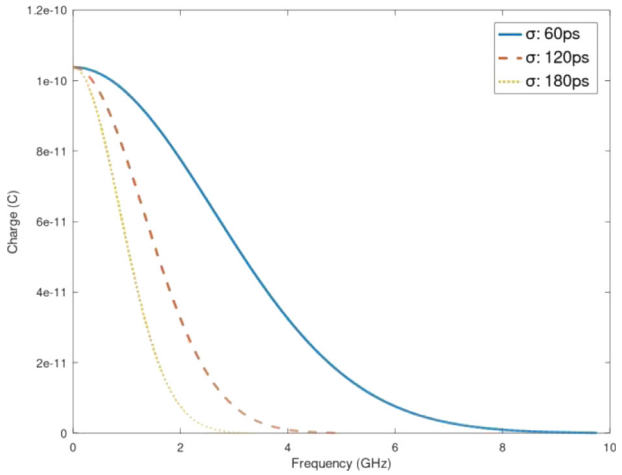


**Fig. 7.** Single bunch frequency spectrum variation with the bunch length.

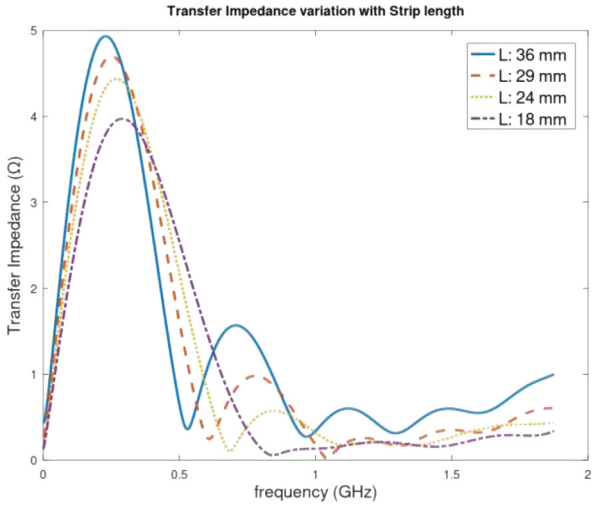


**Fig. 8.** Transfer impedance of the stripline BPM with various electrode lengths.

Fig. 5 shows the transfer impedance of the matched stripline in comparison with the shorted stripline and button pickups with multibunch effects at RF harmonics. In particular for low velocity beams, when the bunch length is relatively large for a short stripline, the signals of consecutive bunches are not separated and have head–tail overlapping. This overlapping produces difference in transfer impedance of single bunch and multibunch of the BPM pickups.

## 4. Matched stripline design

The proton bunches passing through the eight BPMs distributed within MEBT section vary in length at different locations. The *rms* bunch length has a maximum of 0.18 ns in a location near center of MEBT, while has a minimum of 0.06 ns at the end of MEBT (see Fig. 6). This variation in the bunch length, changes frequency spectrum content of the beam in different MEBT locations (Fig. 7). Therefore, the BPMs generate slightly different signal amplitudes at different physical locations of the MEBT (Eqs. (3)–(5), Fig. 9). This is also true for the timing extension of the signal, which reaches out of the BPM electrodes due to variation in frequency components.

The Low-$\beta$ beam simulation results are shown in the Figs. 8, 9. Fig. 8 shows the transfer impedance for a single bunch analysis of the stripline pickups with various lengths of strips from 18 mm to 36 mm.

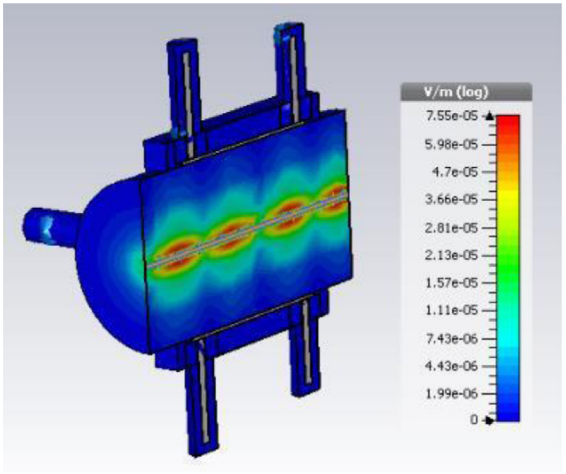


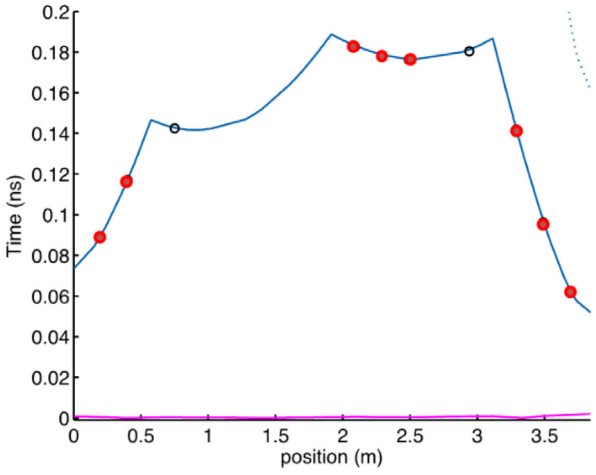


**Fig. 6.** 3D simulation snapshot for low-$\beta$ beam of a centered beam (left), and BPM longitudinal distribution along the MEBT (right). The magenta line represents beam centroid, blue lines represent RMS beam size, red circles represent center of quadrupoles hosting BPMs. (For interpretation of the references to color in this figure legend, the reader is referred to the web version of this article.)

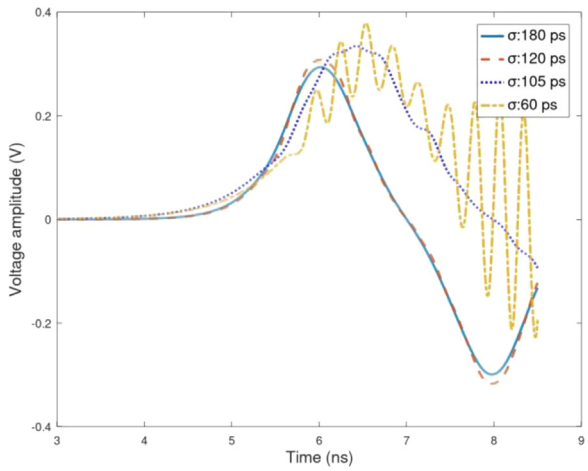


**Fig. 9.** BPM time domain response to a single bunch for various bunch lengths in MEBT.

The plots show the variation of transfer impedance with the frequency. Fig. 9 shows the time domain response of the stripline pickup to a single bunch with various bunch lengths.

The length of electrode pickup is 36 mm between the pin center holes. The electrode length is a tradeoff between the signal power and the overall flange to flange mechanical restriction of the BPM. At the electrode length of 36 mm, the transfer impedance has a peak of 1.6 Ω at 2nd RF harmonic and has a transfer impedance of 4.5 Ω at RF frequency of 352 MHz. All these relations assume that RF matching of the structure including the electrode is already met, and the beam induced signal is leaving out to the cables without mismatch loss.

## 5. BPM manufacturing

After finalizing the electromagnetic simulation and mechanical drawings, several fabrication processes have been studied.

The BPM sensor is composed of several components, which are separately machined and then welded together by the use of electron beam welding. Fig. 10 shows the several parts that compose the sensor, including striplines, RF rectangular boxes to house the striplines and feedthroughs (Fig. 11), ceramic spacers and BPM central tubes. The spacers material is alumina 95% Al2O3 and they are machined to the design dimensions at *Steelceram* [13]. Furthermore, the metallic parts are machined with tolerances of around 10 μm in a local company *Inmepre* [14]. In the second step, the e-beam welding process of various parts has been performed in ESS-Bilbao welding facility. The main welded parts include welding the feedthroughs to RF box, welding the striplines to feedthrough pins, welding the RF boxes to the central tube, welding the bellows to the central tube, welding the flanges to the central part and bellow. During the welding process, thorough RF and vacuum leak checks have been carried out. The RF measurements played a vital role in the process of the fabrication. The idea was to group the RF boxes in families of 4 units, in order to have the four RF boxes of one BPM set, as similar as possible in terms of the impedance matching and losses. The final step was to weld the RF boxes, bellows and flanges to the central BPM tube. The final checks of UHV, RF and magnetic checks were performed before installation of the BPMs inside quadrupoles. Before the fabrication and welding of the final BPMs, several prototypes have been manufactured to check the metrology, vacuum and RF compatibility. In this process, some of the RF boxes have been rejected due to their s-parameters values.

Some of the MEBT BPM sensors have different flange-to-flange length. Within the eight (8) BPMs , there are five (5) types different in overall length. In addition, four BPM types have a bellow, while one type (BPM type 3) does not include bellow. All the MEBT BPMs have DN40 CF rotatable flanges on both sides, except the last BPM (BPM type 5) which has a DN63 CF at the exit side, in order to attach the MEBT to the rest of accelerator in DTL side. (see Fig. 12).

For the installation of BPM, the upper half of the quadrupole has to be removed and after placement and rough alignment of the BPM, the upper part of quadrupole is returned to its place. The final BPM alignment is planned to be performed with Beam Based Alignment (BBA) method [15,16]. By design, the BPMs longitudinal center (i.e. center of RF box) are located on the longitudinal center of quadrupole magnets. Patch panels have been installed on the MEBT support, in order to facilitate the access to the BPM outputs and interchange the 120 cm-long, small diameter coaxial cables with SMA connectors to 50 m-long, large diameter coaxes with N connectors. The short cables have been

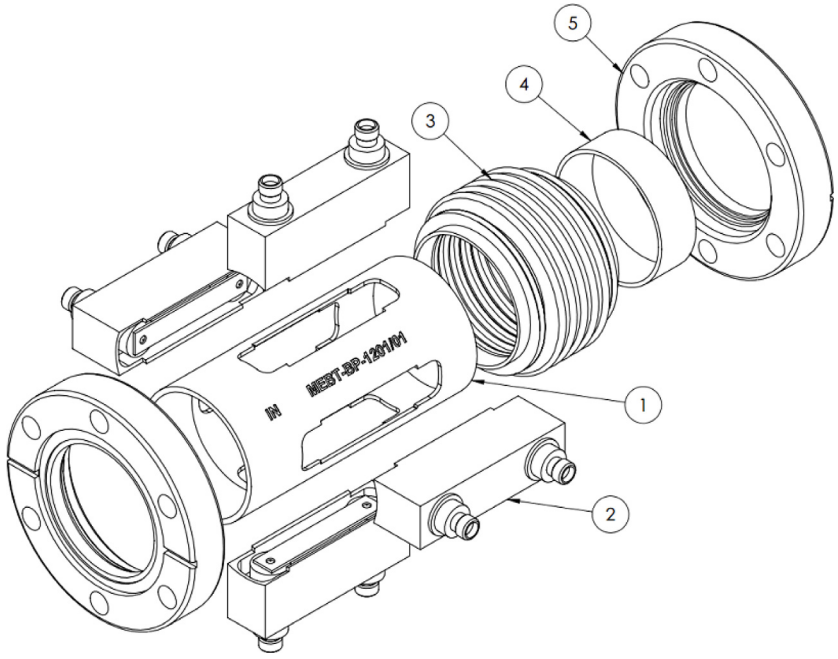


**Fig. 10.** Details breakdown of pieces of one BPM with bellow includes BPM tube(1), RF box(2), Bellow(3), length adjustment tube(4) and CF flange(5).

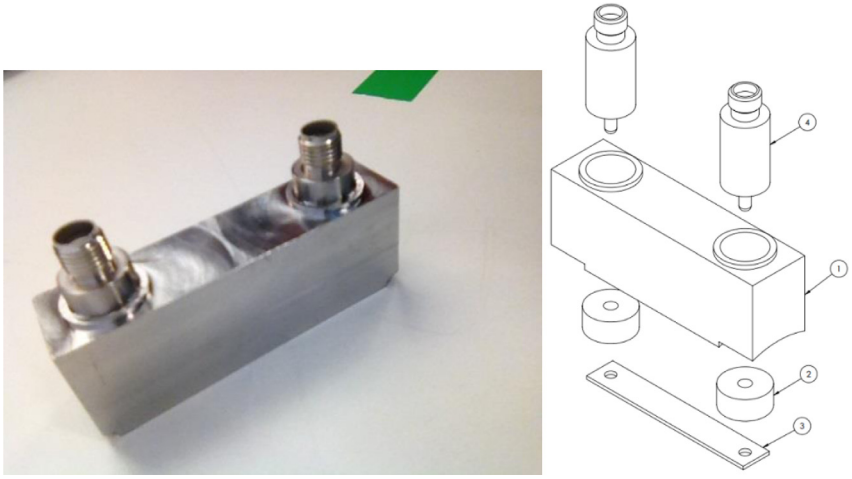


**Fig. 11.** One RF box ready for the s-parameters measurements before welding to the BPM tube (left) and the breakdown of pieces(right) showing RF housing box(1), alumina spacer(2), strip(3) and feedthrough(4).

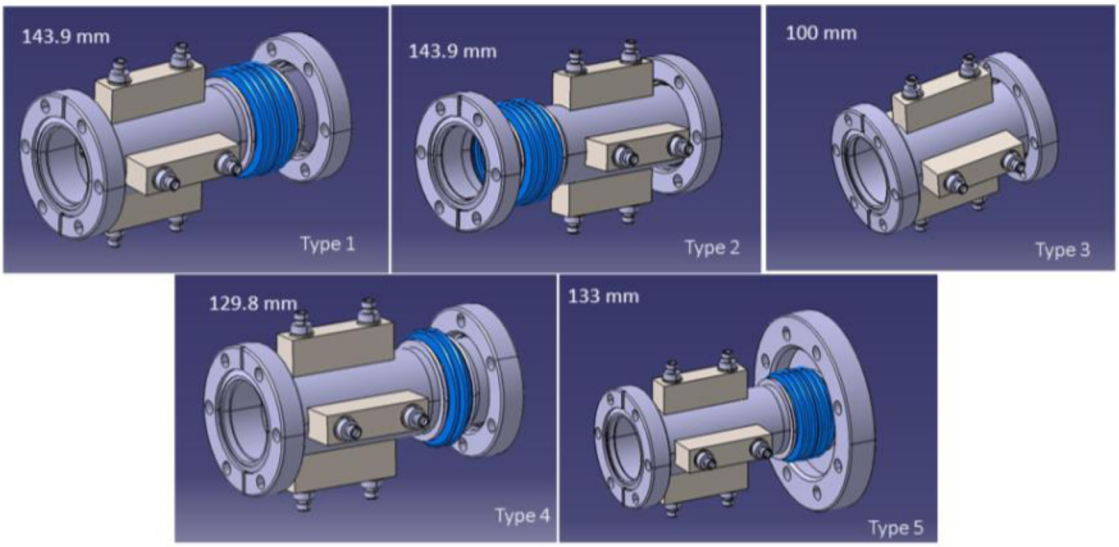


**Fig. 12.** Various types of BPMs of the MEBT.

**Table 2**
BPM types and corresponding quadrupoles.

| BPM | BPM1 | BPM2–1 | BPM2–2 | BPM2–3 | BPM3–1 | BPM3–2 | BPM4 | BPM5 |
|---|---|---|---|---|---|---|---|---|
| Quad. | Q2 | Q3 | Q5 | Q9 | Q6 | Q10 | Q7 | Q11 |
| Type | BPM1 | BPM2 | BPM2 | BPM2 | BPM3 | BPM3 | BPM4 | BPM5 |
| Length (mm) | *143.9* | *143.9* | *143.9* | *143.9* | *100* | *100* | *129.8* | *133* |

assembled with electrical length difference of less than 10 ps, in order to keep the phase variation of BPM pick-ups in the required limit. The coaxial cables are fire resistant, halogen free and have the LSZH PE jackets. The patch panels include the SMA-N adaptors and attached to the MEBT support in several locations.

The permeability checks show the relative permeability of different points of the BPM set, not larger than 1.07. Table 2 shows various types and length of the BPMs and their corresponding quadrupoles installed in MEBT.

During the fabrication several tools were developed in order to secure the mechanical tolerances of pieces welding. After fabrication of the BPMs, the metrology measurements have been performed by means of 3D CMM method. The horizontal and vertical planes offset errors are within ±150 μm, and the mechanical installation alignment errors are 200 μm (see Fig. 13).

## 6. Electrical measurements

In order to match the impedance of the BPM strips to the coaxial cables and electronics, the BPM reflection coefficients are measured during the prototypes, compared with 3D computer codes, and the dimensions of the BPM structure components including electrode thickness, wall distance of the electrode, feedthrough pin diameter, ceramic spacer dimension are finalized.

During the process of welding and fabrication of the BPMs, several checks including the vacuum leakage, RF, electrical and metrology checks were carried out. The final RF and vacuum checks have been performed just before installation of the BPMs inside quadrupoles and after installation in the MEBT, connecting the BPM cables to the patch panels. Fig. 14 shows the laboratory setup for the RF checks of the BPMs. It includes the network analyzer with two ports for the reflection and transmission coefficients measurement of the BPM sets. In general, the signal port S-parameters are measured with and without 50 Ω termination. The 50 Ω termination is removed for the S12 measurement. For the coupling measurement between adjacent and opposite electrodes,

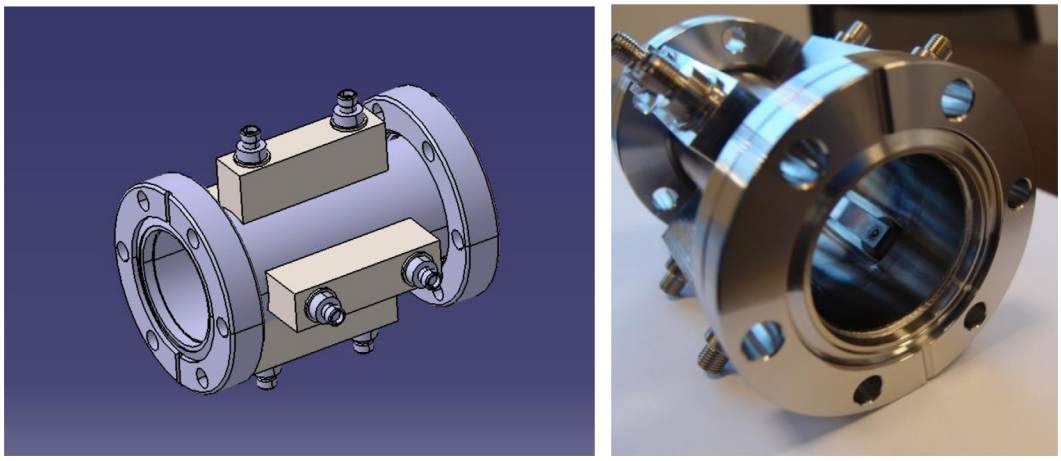

**Fig. 13.** Two views of BPM3 with flange-to-flange length of 100 mm.

**Fig. 14.** One BPM under RF and electrical characterization checks in the laboratory.

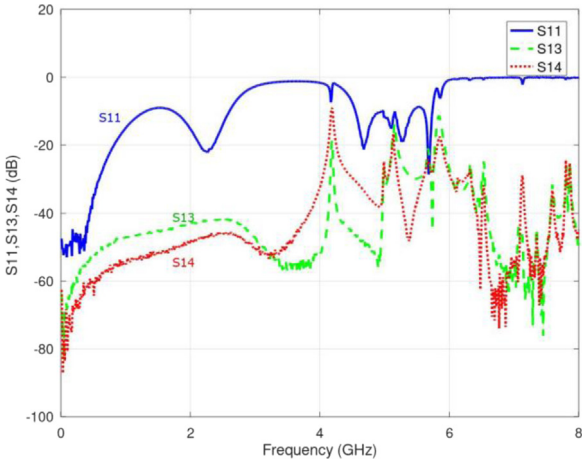


**Fig. 15.** Measured return loss and couplings for BPM3.

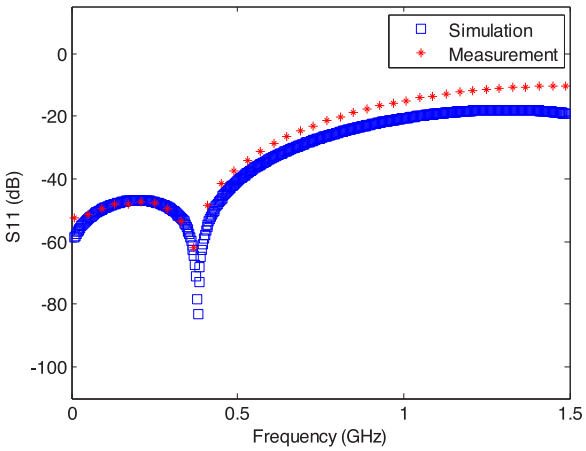


**Fig. 16.** Measured and simulation values of the BPM return loss, S11.

all other ports are terminated with corresponding 50 Ω terminations. Fig. 15 shows the measured S11 return loss (solid line), S13 adjacent strip pick-ups coupling (dashed line) and S14 opposite strip pick-ups coupling for the BPM. The measurements show a return loss of ∼ −21 dB and coupling of around −50 dB for adjacent strip pick-ups (e.g up and left) for all the BPMs at the frequency of 704 MHz. The coupling of opposite strip pick-ups (e.g up and down) is around −58 dB at frequency of 704 MHz. The measured bandwidth (3 dB) of the BPMs is ∼3 GHz.

The s-parameters measurement, unlike the stripline voltage power response, are not affected by the beam velocity. Therefore the laboratory measurements are perfectly corresponding to the BPM structure. Fig. 16 shows the measurement and simulation values of the reflection coefficients. The BPM RF measurements when compared to the simulation results, are more significantly different at higher frequencies since the alumina spacers characteristics, mechanical errors and welding quality are more comparable to the wavelength at higher frequencies, introducing this expected behavior in the results shown in Fig. 16.

Table 3 shows the values of simulation and measurements of the S-parameters of the BPM sensors at the first, second and third harmonics of the RF bunching signal. During the process of electrical measurements, it has been observed abnormal results in some BPM sets. In those BPM sets, the S11 value results of some pickups showed different values

**Table 3**
BPM s-parameters simulation and measurements comparison at RF harmonics.

| Frequency | S11 (dB) | | S13 Adj. coupling (dB) | | S14 Opp. coupling (dB) | |
|---|---|---|---|---|---|---|
| | Simulation | Measurement | Simulation | Measurement | Simulation | Measurement |
| 352 MHz | −52 | −55 | −58.8 | −56.7 | −65.3 | −64.7 |
| 704 MHz | −28.6 | −24.4 | −53.2 | −50.1 | −59.6 | −58 |
| 1.1 GHz | −19.4 | −13.8 | −49.4 | −47.2 | −55.5 | −54.6 |

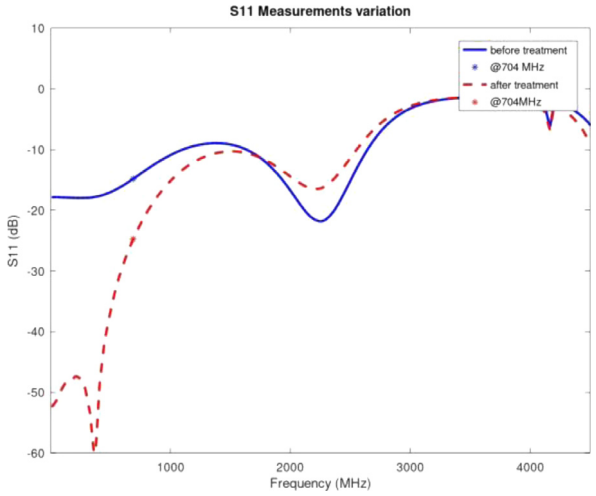


**Fig. 17.** The S11 graphs of one BPM before (solid line) and after (dashed line) the voltage treatment.

than electromagnetic simulations in particular at lower frequencies and DC mode. The thorough analysis of the results showed the possibility of tiny jumpers and residues with approximate thickness/diameters of 2-3 μm between signal path and BPM ground. These could be happened during the welding process of various parts. In order to fix the potential problem, a defusing voltage is used to remove the residues/shorts between the conducting surfaces and the ground surfaces of BPM. After this treatment, new measurements on s-parameters showed the correct values of s-parameters which are expected by simulation. Fig. 17 shows the S11 graph of a BPM before and after defusing voltage treatment.

Furthermore, the electrical off-set of the BPMs strips have been identified with two methods. The first method uses a rigid wire antenna allocated precisely in the center of the BPM tube (around 50 μm error). An RF signal of 704 MHz are passing through the antenna and the signals on the stripline pick-ups are measured with an spectrum analyzer. From the difference between pick-up signals and by introducing the position sensitivity values, the x/y planes offsets have been identified. The other method is the so-called "Lambertson" method which measures the electrical off-sets from the s-parameters of the stripline pick-ups [17,18]. It is based on the simultaneous measurement of BPM four pick-ups with network analyzer and analyzing the data in order to identify the x/y planes off-sets. The measurements in both methods show an off-set of smaller than ±175 μm in x/y planes. Due to integration of the BPMs inside quadrupoles and the critical importance of the inner/outer surfaces and dimensions, 3D metrology measurement with CMM machine for all BPMs have been realized at a local center for advanced fabrication- *CFAA* [19]. In those measurements, the linear dimensions, angles, flatness and distances of critical parts of the BPMs have been measured. From the measurement data, the mechanical off-sets of x/y planes are found smaller than ±150 μm. The fine alignment of the 8 BPMs of the MEBT will be realized based on Beam Based Alignment method (BBA) using the corresponding quadrupole magnets.

## 7. Thermal effects on RF charcteristics

The thermal sensitivity of the BPM reflection coefficients is another measurement which is performed after fabrication of the BPM sensors.

**Table 4**
S11 and Coupling thermal sensitivity of BPM.

| Coefficient @704 MHz | Sensitivity dB/°C |
|---|---|
| S11 | −0.0075 |
| S13 (adjacent coupling) | 0.0156 |
| S14 (opposite coupling) | 0.011 |

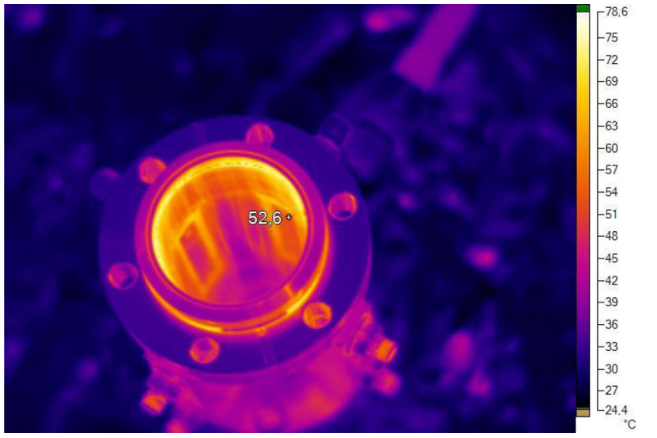


**Fig. 18.** A BPM set under thermal effects measurements.

In this measurement, the BPM pickups connected to the network analyzer, are thermally heated by a blower up to 55 °C. The temperature on the pickup surfaces are measured with a thermal camera (Fig. 18). The s-parameter development with temperature was characterized at frequency of 704 MHz.

In particular this check was essential for the BPM sets of MEBT, in which the internal aperture is relatively small and in some areas after beam chopper, there is a probability of thermal heat of vertical pickups in abnormal situations. In order to reduce the probability of beam hitting the strips, the BPM pipe diameter in the beam entrance is slightly smaller than the exit diameter (D36.8 mm vs. D37.8 mm), while the radial distance of the opposite strips is kept as 37.8 mm. In the MEBT, the quadrupole between the MEBT chopper and its beam dump, does not include any BPM stripline. At this location, the chopped beam is vertically deflected, and the accumulation of heat on strips due to possible deflection error could damage the BPM strips.

Table 4 shows the value of return loss, adjacent and opposite pick-ups couplings. The sensitivity values are relatively small. The values for a 20 °C temperature variation, correspond to variations of 0.015 dB, 0.3 dB and 0.2 dB for S11, S13 and S14 accordingly.

## 8. Measurement with the IPHI beam

The BPM system is composed by several components other than the BPM sensor. These additional building blocks of the system are composed by hardware and software designs that allow beam phase and position measurements to be performed in the accelerator. The signal is excited to the BPM striplines through the beam image current in the vacuum chamber, which is then transmitted through low phase drift cables, then processed by front-end electronics and is then digitized in subsequent stage. A digital signal processing is performed real-time in an FPGA that runs in a MicroTCA.4 crate [6].

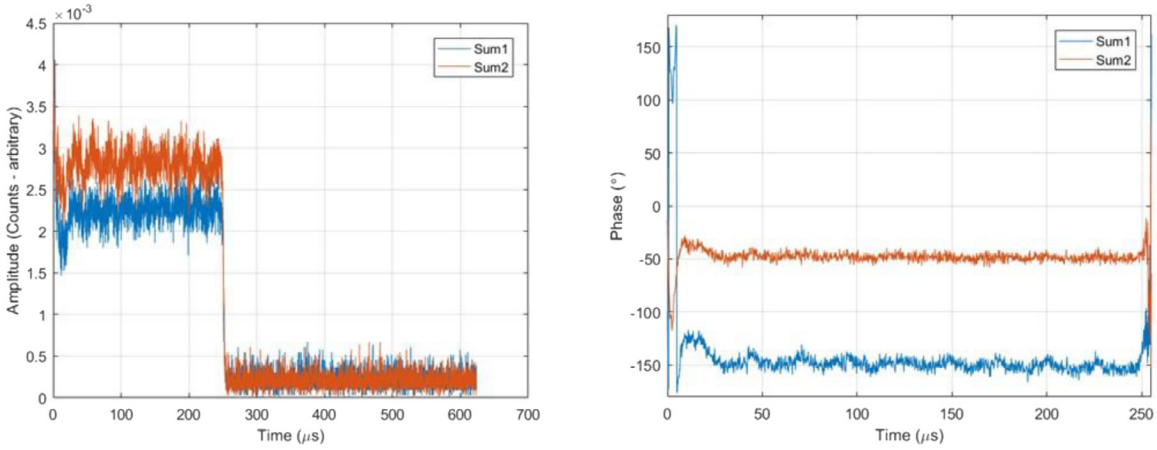


**Fig. 19.** Beam amplitude and phase along the pulse.

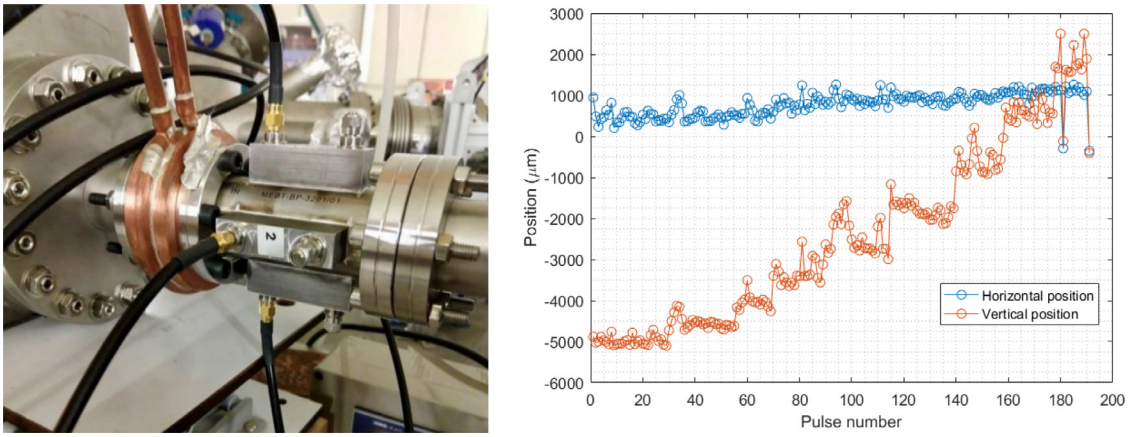


**Fig. 20.** BPM installed and protected with collimator for vertical test at IPHI beamline (left) and horizontal/vertical beam position changes for 30 consecutive pulses.

The proton beam characteristics during the tests have been changed to allow a scan of the parameters that could replicate the ESS beam. Beam energy was set to 3 MeV, defined by the RFQ settings. Beam current has been varied from 0.4 mA and 50 mA by changing the iris aperture and the pulse length has been changed from 150 μs up to 3 ms. A phase reference line is generated with an external RF generator locked to the RF system of the RFQ in order to allow locked phase measurements of the beam. The BPM signal processing chain is composed by several stages that are able to provide user with information in different bandwidths. The first data stream stage provides the user with ADC raw data sampled at 88 MHz from all the 4 striplines and the reference line followed by a near-IQ processing which provides baseband decimated amplitude and phase measurements. Further amplitude and phase processing is performed to provide beam position and beam phase relative to reference line.

For a single pulse, amplitude data is used to monitor the beam location in time domain by the use of a self-trigger functionality that starts the acquisition when an amplitude threshold is reached. The amplitude of the signal is dependent on the bunch length at the BPM location and the beam current, which then excites the second harmonic of the signal. Fig. 19 shows an example of an intra-pulse measurement of the amplitude signal and beam phase measurements.

The beam position has been measured during a beam steering experiment in the accelerator where the beam is moved from −5mm to 2 mm in the vertical orientation (Fig. 20).

Beam phase has been measured during the mentioned experiment using a pair of BPM sensors. The ESS MEBT BPM has been used for phase measurements together with an existing CEA button BPM, which

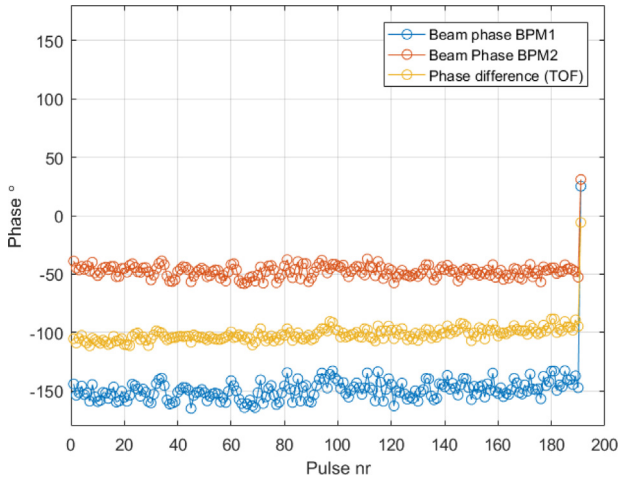


**Fig. 21.** Beam phase measurements in the ESS BPM in comparison to the CEA button BPM.

was already in operation in the machine [20]. Both measurements are shown in Fig. 21 and have been performed for 10 mA, 500 us pulse width and 200 consecutive pulses. The pulse-to-pulse measurement fluctuations were observed in both BPM systems and are due to the measurement noise and pulse-to-pulse beam characteristics of the

machine. This has been confirmed with data from other existing BPM systems in the machine and using a different data acquisition system.

The beam phase measurements on each BPM are obtained by measuring the phase of the beam in each individual BPM and then compared to the phase of the RF signal that is provided by the reference signal, in a phase locked loop (PLL) with the RF system of the CEA accelerator. The additional phase noise added by the phase generation circuit in a bandwidth from 100 Hz to 10 MHz, is less than 1 ps. The phase of each BPM is obtained by comparing the same digitized reference signal, meaning that no absolute phase errors are introduced by the reference signal.

The phase of each BPM is then compared to each other to provide the phase difference, or time-of-flight (TOF) of the beam. The TOF is shown in Fig. 21 to demonstrate that over several minutes of acquisition the pulse to pulse phase correlation between the measurements is high when we compare the phase measurements of the ESS MEBT BPM and the CEA button BPM.

## CRediT authorship contribution statement

**S. Varnasseri:** Writing - original draft, Methodology, Software. **I. Bustinduy:** Supervision. **I. Rueda:** Investigation. **R.A. Baron:** Writing - review & editing. **A. Ortega:** Visualization. **A. Zugazaga:** Data curation. **A. Conde:** Validation. **J. Martin:** Validation. **T. Shea:** Project administration.

## Declaration of competing interest

The authors declare that they have no known competing financial interests or personal relationships that could have appeared to influence the work reported in this paper.

## Acknowledgments

The BPM measurements campaign with IPHI beam has received funding from the European Union's Horizon 2020 Research and Innovation program under Grant Agreement No 730871. The authors thank the IPHI team from the Division of Accelerators, Cryogenics and Magnetism during the measurements at CEA — Saclay. We would like to thank Akihiko Miura (J-PARC/JAEA), A.V Alexandrov (ORNL), and our colleagues H. Hassanzadegan (ESS), D. Fernandez-Cañoto, J.L Muñoz (ESS-Bilbao) and I. Podadera (CIEMAT) for the fruitful discussions.

## References

[1] R. Garoby, et al., The European spallation source design, Phys. Scr. 93 (2018) 014001.
[2] K.H. Andersen, et al., The instrument suite of the European Spallation Source, Nucl. Instrum. Methods 957 (2020) 163402.
[3] ESS ERIC, https://europeanspallationsource.se.
[4] A. Jansson, et al., Beam diagnostics for ESS commissioning and early operation, MOPMR020, Proc. IPAC 2016, pp. 273–275.
[5] P. Forck, P. Kowina, D. Liakin, Beam Position Monitors, in: CERN Accelerator School: Beam Diagnostics, Dourdan, France, 2009.
[6] R. Baron, et al., ESS beam position and phase monitor system, in: WEPP015, Proc. IBIC, 2019, pp. 543–547.
[7] R. Miyamoto, et al., Highlights from the first beam commissioning stage at ESS for its ion source and low energy beam transport, JINST 15 (2020) P07027.
[8] R. Miyamoto, M. Eshraqi, M. Muños, C. Plostinar, Beam Commissioning Planning Updates for the ESS Linac, in: TUPVA131, Proc. IPAC, 2017, pp. 2407–2410.
[9] D. Fernandez Cañoto, et al., Quadrupole magnet design for ESS MEBT, in: THPIK082, Proc. IPAC, 2017, pp. 4276–4278.
[10] R.E. Shafer, Beam Position Sensitivity for low-$\beta$ beams, in: Proc. International Linac Conference, 1994, pp. 905–907.
[11] R.E. Shafer, Characteristics of directional coupler beam position monitors, IEEE Trans. Nucl. Sci. NS-32 (5) (1985) 1933–1937.
[12] J.H. Cuperus, Monitoring of particle beams at high frequencies, Nucl. Instrum. Methods 145 (1977) 219.
[13] Steelceram, www.steelceram.com.
[14] Inmepre, www.inmepre.com.
[15] P. Roejsel, A beam position measurement system using quadrupole magnets magnetic centra as the position reference, Nucl. Instrum. Methods 343 (1994) 374.
[16] C.E. Adolphsen, et al., Beam-Based Alignment Technique for the SLC Linac, SLAC-PUB-4902, 1989.
[17] G.R. Lambertson, Calibration of Position Electrodes using External Measurements, LSAP Note-5, LBL, 1987.
[18] Y. Chung, G. Decker, Offset calibration of the Beam Position Monitor Using External Means, AIP Conf. Proc. 252 (1992) 217.
[19] CFAA, https://www.ehu.eus/es/web/CFAA.
[20] Maurice Cohen-Solal, Design, test, and calibration of an electrostatic beam position monitor, Phys. Rev. ST Accel. Beams 13 (2010) 032801.